Advances in Nano Research, *Vol. 12, No. 6 (2022) 593-603*
https://doi.org/10.12989/anr.2022.12.6.593

Thermal buckling resistance of a lightweight lead-free piezoelectric nanocomposite sandwich plate

Kamran Behdinan* and Rasool Moradi-Dastjerdi[a]

Advanced Research Laboratory for Multifunctional Lightweight Structures (ARL-MLS), Department of Mechanical & Industrial Engineering, University of Toronto, Toronto, Canada

(*Received December 12, 2021, Revised February 23, 2022, Accepted March 16, 2022*)

Abstract. The critical buckling temperature rise of a newly proposed piezoelectrically active sandwich plate (ASP) has been investigated in this work. This structure includes a porous polymeric layer integrated between two piezoelectric nanocomposite layers. The piezoelectric material is made of a passive polymeric material that is activated by lead-free nanowires (NWs) of zinc oxide (ZnO) embedded inside the matrix. In both nanocomposite layers and porous core, functional graded (FG) patterns have been considered for the distributions of ZnO NWs and voids, respectively. By adopting a higher-order theory of plates, the governing equations of thermal buckling are obtained. This set of equations is then treated using an extended mesh-free solution. The effects of plate dimensions, porosity states, and the nanowire parameters have been investigated on the critical buckling temperature rises of the proposed lightweight ASPs with different boundary conditions. The results disclose that the use of porosities in the core and/or mixing ZnO NWs in the face sheets substantially arise the critical buckling temperatures of the newly proposed active sandwich plates.

Keywords: active sandwich plates; piezoelectric nanocomposite; porous material; thermal buckling; zinc oxide nanowires

1. Introduction

Innovative lightweight structures are widely used for various purposes such as engineering structures and biomedical devices (Sobhani *et al*. 2022b). From the mechanical point of view, the key factor in the design of such structures is the strength-to-weight ratio where the ordinary use of lighter materials results in massive reductions in structural stiffness (Behdinan and Moradi-Dastjerdi 2021, Sobhani and Masoodi 2021, Sobhani *et al*. 2021). To compensate for this strength diminution, involving multifunctional materials or improving the structural design can be beneficial solutions (Foroutan and Moradi-Dastjerdi 2011, Pan *et al*. 2021, Safaei 2021, Ghahramani *et al*. 2022, Sobhani *et al*. 2022a). Composites/ nanocomposites and foams are some examples of multifunctional lightweight materials that their combined uses in sandwich structures can meet the needs for an advanced structure with a high strength-to-weight ratio (Alian *et al*. 2015, Wang *et al*. 2018, Zargar *et al*. 2019, Zhao *et al*. 2020, Moradi-Dastjerdi and Behdinan 2021c). In these sandwich structures, a thick layer made of a softer and lighter material is integrated between two far thinner layers made of a stiffer material where the proper selection of each layer can significantly change the failure mode of the whole sandwich structures (Tao and Dai 2022). Moreover, as demands for smart structures are growing, novel sandwich structures activated with involving piezoelectric materials are extensively proposed to make them capable of generating electrical signals from mechanical deflections or vice versa (Moradi-Dastjerdi and Behdinan 2021b). These exceptional capabilities create so many applications for such active sandwich structures such as noise/vibration suppression (Kundalwal and Ray, 2016), harvesting clean energies (Keshmiri *et al*. 2018, Malekzadeh *et al*. 2018, Setoodeh *et al*. 2018, 2019, Moradi-Dastjerdi and Behdinan 2021a, Zhang *et al*. 2022), fuel or drug delivery micropumps (Angelou *et al*. 2021), and structural deformation monitoring (Tuloup *et al*. 2019). The design and characterization of such piezoelectrically active structures are still needed to be precisely investigated given the fact that they deal with advanced materials and small-scale deflections/electrical charges.

Due to the significance of thermal buckling analysis in innovative structures, especially thinner ones, this type of analysis has been considered for new lightweight structures made of foams, composites, nanocomposites, etc., in recent works (Yang *et al*. 2022). Singh *et al*. (2013) extended a collocation mesh-free solution to characterize buckling temperature and forces laminated composite plates. Cetkovic (2016) considered the same plates and presented buckling temperature using a layerwise theory and isoparametric FEM. Laminated composite beams also were subjected to study their buckling temperature, moisture, and forces using a hyperbolic refined theory (Bouazza and Zenkour 2020). By developing an isogeometric FEM method, buckling temperatures of FG ceramic/metal blades and nanoplates with arbitrary shapes were presented in (Malekzadeh *et al*. 2011, Ansari and Setoodeh 2019). Likewise, porous and/or nanocomposite materials as lightweight structures have

*Corresponding author, Professor,
E-mail: behdinan@mie.utoronto.ca
[a] Ph.D., Email: moradi@mie.utoronto.ca

ISSN: 2287-237X (Print), 2287-2388 (Online)

been subjected to study their buckling performances. Mirzaei and Kiani (2017) developed an isogeometric FEM to investigate buckling temperatures of plates made of graphene-enhanced laminated composites. They also assumed that the material properties of the utilized composite are temperature dependent. Buckling temperatures of curved CNT-reinforced shells with FG patterns of CNT distributions were calculated using a FEM formulation and considering a multiscale approach (Mehar *et al*. 2019). Buckling temperatures of ultra-thin nanoplates with considering viscoelasticity of the plates were presented using nonlocal theory (Sobhy and Zenkou 2018). Jabbari *et al*. (2014) theoretically analyzed buckling temperatures of circular foam plates with various FG profiles of void distributions. These porous plates with rectangular shapes were also considered to evaluate their buckling temperatures using a quasi 3D theory (Mekerbi *et al*. 2019). Buckling temperatures of microscale beams with embedded porosities along 2D-FG patterns were numerically studied using Euler–Bernoulli theory by Mirjavadi *et al*. (2017). Using an isogeometric analysis based on an advanced theory, Fan *et al*. (2021) conducted a nonlinear analysis to present postbuckling temperatures of FG porous nanoplates with a square cutout. For double-walled CNTs, thermal buckling temperatures were investigated using a nonlocal theory and Timoshenko beam model (Tounsi *et al*. 2013). Arshid *et al*. (2021b) considered circular nanoplates with embedded graphene particles and voids and studied the thermal buckling of this lightweight nanostructure using a numerical approach. Furthermore, for sandwich plates with FG ceramic/metal and homogeneous layers, a nonlinear theoretical study was performed to present buckling temperatures and forces (Trinh and Kim 2019). The effect of accommodating porosities into the same sandwich structures on the nonlinear buckling responses was also investigated using a higher-order theory (Cong *et al*. 2018). Kamarian *et al*. (2020, 2021) considered a soft-core plate sandwiched between nanocomposite / composite layers, and studied buckling behaviors of the resulting sandwich plates. Moreover, a sandwich cylinder with FG porous core located inside an elastic medium was also investigated to obtain its buckling temperature in a framework of a nonlinear study (Ahmadi and Foroutan 2020).

Turning to active structures which involve piezoelectric layers or patches, the study of their buckling temperature was also subjected in only a few numbers of recent research works. For example, laminated composite plates sandwiched between piezoelectric layers were subjected to study the piezoelectric effect on the buckling temperature using an extended 3D-FEM (Akhras and Li 2010). In an analytical work, buckling temperatures of FG ceramic/metal plates integrated between piezoelectric faces were studied while the material properties of the substrate layer were temperature-dependent (Yaghoobi *et al*. 2015). For FG ceramic/metal thin-walled cylinders with an outer piezoelectric layer, buckling temperatures were analytically calculated (Dinh Khoa *et al*. 2019). Moreover, buckling temperatures of piezoelectric nanoplates lightened with involving porosities were investigated using Navier's method (Zenkour and Aljadani 2019). These nanoplates were made of FG distributions of two different piezoceramics. By developing a nonlocal theory, the buckling behavior of nanoscale piezoelectric beams subjected to a multi-physics environment was studied (Ebrahimi *et al*. 2016, 2018). This non-classic theory is also utilized for the investigation of buckling resistance of nanoscale CNT-reinforced plates actuated by piezoelectric materials (Heidari *et al*. 2020). As another form of active lightweight structure, Sobhy (2021) considered passive substrates made of FG foams and auxetic structures sandwiched between two FG piezoceramic layers. He presented buckling temperature for such active lightweight structures. Advanced lightweight sandwiches of FG porous and FG nanocomposite were also activated by piezoceramic layers and their buckling temperatures and forces were obtained numerically in (Moradi-Dastjerdi and Behdinan, 2020a). However, the active layers (piezoceramics) of the aforementioned structures include lead which is a hazardous material. To address this issue, the use of some forms of lead-free piezoelectric materials in mechanical structures has been suggested (Mishra *et al*. 2017, Meschino *et al*. 2021). Mosallaie Barzoki *et al*. (2012) passive polyethylene foam cylinders activated by an outer piezoelectric PVDF layer with embedded piezoelectric boron nitride nanotubes. They presented buckling torsional load for their proposed active cylinders. Moreover, Arshid *et al*. (2021a) considered FG porous nanoplates bounded between two lead-free active layers made of piezoelectric PVDF with embedded passive carbon nanotubes and presented buckling forces using non-classical mechanics.

As it was reviewed in the literature, the thermal buckling behavior of active structures made of lead-free piezoelectric materials has not been investigated yet. Therefore, in this paper, first, an advanced lightweight active structure is suggested such that the structure consists of an FG porous polymeric plate activated by piezoelectric polymeric nanocomposite layers with FG dispersions of ZnO NWs. Then, the critical buckling temperature of the suggested lightweight ASP is characterized where the governing eigenvalue system of equations is obtained and treated by extending a mesh-free solution based on a higher-order theory.

2. Modeling of the ASP

Lightweight active sandwich plates consisting of one passive porous layer and two nanocomposite piezoelectric layers have been considered in this work. The active layers of these ASPs are made of piezoelectric nanowires of ZnO embedded in a passive polymeric matrix while the passive core is a porous polymeric layer. By considering a uniform environment temperature, the critical buckling temperatures for such ASPs have been investigated. As depicted in Fig. 1, the inner faces of the piezoelectric layers are grounded while the outer ones are left electrically free (open circuit). The geometrical dimensions of the APS are also described in Fig. 1.

2.1 Material properties

For further lightening of the proposed ASP, the use of a

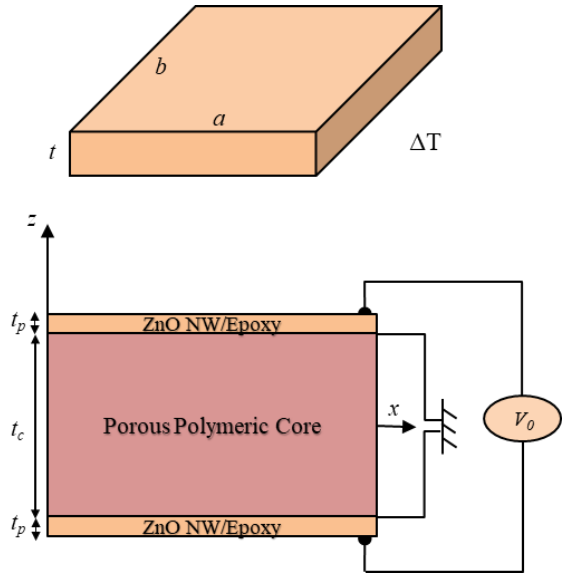

Fig. 1 Dimensions and electrical boundary condition of the lightweight active sandwich plates

porous polymeric layer has been selected for the core of these sandwich plates. Moreover, to investigate the effect of void distribution, symmetric and uniform patterns of distributions along the thickness of the core layer have been considered while the amount of void is similar in both patterns. The density ρ^c and young's modulus of E^c the porous material can be evaluated as follows (Nguyen *et al*. 2019, Moradi-Dastjerdi *et al*. 2020):

$$\text{Uniform: } \rho^c = \left(\frac{2}{\pi}\sqrt{1-p_0} - \frac{2}{\pi} + 1\right)\rho \ , \quad E^c = \left(\frac{2}{\pi}\sqrt{1-p_0} - \frac{2}{\pi} + 1\right)^2 E \tag{1}$$

$$\text{Symmetric: } \rho^c = \left(1 - p_m \cos\left(\frac{\pi z}{t_c}\right)\right)\rho \ , \quad E^c = \left(1 - p_0 \cos\left(\frac{\pi z}{t_c}\right)\right)E \tag{2}$$

where p_0 which represents the void amount is porosity parameter, ρ is the density of a nonporous core, E is young's modulus of a nonporous core, and $p_m = 1 - \sqrt{1-p_0}$. According to Eqs. (1)-(2), there is no porosity in the core when $p_0 = 0$. Poisson's ratio of the porous core v^c is also evaluated as below:

$$v^c = 0.221\beta + v(0.342\beta^2 - 1.21\beta + 1) \ , \ \beta = 1 - \frac{\rho^c}{\rho} \tag{3}$$

where $\beta < 0.7$ (Polit *et al*. 2019). Moreover, the thermal expansion coefficient of this porous layer α^c has been evaluated using the same equation employed for E^c.

As mentioned earlier, the nanocomposite layers contain specific amounts of ZnO NWs mixed in a polymeric matrix. The physical (mechanical and piezoelectric) properties of these layers have been evaluated using an electro-mechanical model described in (Tan and Tong 2001). To investigate the impact of the dispersion of these active nanowires on the thermal buckling behavior of the proposed ASP, different FG patterns were also considered for the distribution of ZnO NWs along with the thickness of face sheet layers. These FG patterns are described by the volume fraction of ZnO NWs f_r as follows (Moradi-Dastjerdi and Behdinan, 2020b):

$$\text{Top face sheet: } f_r(z) = \left[1 + (2z - t)/2t_p\right]^{\lambda} f_0 \tag{4}$$

$$\text{Bottom face sheet: } f_r(z) = \left[1 - (2z + t)/2t_p\right]^{\lambda} f_0 \tag{5}$$

where the exponent λ and the specific nanowire volume fraction f_0 control the distribution profile of ZnO NWs.

2.2 Governing equations

In this work, the displacement field is determined using a higher-order theory that has only five unknowns (degrees of freedom). Reddy established this advanced theory such that displacement modules (u, v and w) were defined as (Reddy, 2004):

$$\begin{aligned} u &= u_0(x,y) + z\theta_x(x,y) + z^3 c_1\left(\theta_x + w_{0,x}\right) \\ v &= v_0(x,y) + z\theta_y(x,y) + z^3 c_1\left(\theta_y + w_{0,y}\right) \\ w &= w_0(x,y) \end{aligned} \tag{6}$$

where u_0, v_0, and w_0 are mid-plane displacements, and θ_x and θ_y are mid-plane rotations. The coefficient c_1 is also $c_1 = \frac{-4}{3t^2}$.

According to Eq. (6), in-plane $\boldsymbol{\varepsilon}_b$ and out of plane $\boldsymbol{\gamma}$ strain vectors are obtained as (Reddy 2004, Moradi-Dastjerdi and Behdinan 2021d):

$$\boldsymbol{\varepsilon}_b = \boldsymbol{\varepsilon_0} + z\boldsymbol{\varepsilon}_1 + c_1 z^3 \boldsymbol{\varepsilon}_3, \boldsymbol{\gamma} = (1 + 3c_1 z^2)\boldsymbol{\gamma}_0 \tag{7}$$

where

$$\boldsymbol{\varepsilon_0} = \begin{Bmatrix} u_{0,x} \\ v_{0,y} \\ u_{0,y} + v_{0,x} \end{Bmatrix}, \boldsymbol{\varepsilon}_1 = \begin{Bmatrix} \theta_{x,x} \\ \theta_{y,y} \\ \theta_{x,y} + \theta_{y,x} \end{Bmatrix}, \quad \boldsymbol{\varepsilon}_3 = \begin{Bmatrix} \theta_{x,x} + w_{0,xx} \\ \theta_{y,y} + w_{0,yy} \\ \theta_{x,y} + \theta_{y,x} + 2w_{0,xy} \end{Bmatrix}, \boldsymbol{\gamma}_0 = \begin{Bmatrix} \theta_x + w_{0,x} \\ \theta_y + w_{0,y} \end{Bmatrix} \tag{8}$$

To capture the piezoelectric effect, the constitutive equations for these active materials are defined as coupled electromechanical equations such that the vectors of mechanical stress $\boldsymbol{\sigma}$ and electrical displacement $\boldsymbol{D}$ are described using vectors of strains $\boldsymbol{\varepsilon}$ and electric field $\boldsymbol{E}$ and matrices of elastic stiffness $\boldsymbol{Q}$, dielectric constants $\boldsymbol{k}$, and piezoelectric constants $\boldsymbol{e}$ as follows (Mosallaie Barzoki *et al*. 2012):

$$\begin{cases} \boldsymbol{\sigma} = \boldsymbol{Q\varepsilon} - \boldsymbol{e}^T\boldsymbol{E} \\ \boldsymbol{D} = \boldsymbol{e\varepsilon} + \boldsymbol{kE} \end{cases} \tag{9}$$

where (Moradi-Dastjerdi and Behdinan 2021d):

$$\boldsymbol{\sigma} = \{\boldsymbol{\sigma}_b \quad \boldsymbol{\sigma}_s\}^T, \boldsymbol{\sigma}_b = \{\sigma_{xx} \quad \sigma_{yy} \quad \tau_{xy}\}^T, \boldsymbol{\sigma}_s = \{\tau_{yz} \quad \tau_{xz}\}^T \tag{10}$$

$$\boldsymbol{\varepsilon} = \{\boldsymbol{\varepsilon}_b \quad \boldsymbol{\gamma}\}^T \tag{11}$$

$$\boldsymbol{Q} = \begin{bmatrix} \boldsymbol{Q}_b & 0 \\ 0 & \boldsymbol{Q}_s \end{bmatrix} \tag{12}$$

$$\boldsymbol{E} = -\{0 \quad 0 \quad V_z\}^T \tag{13}$$

$$\boldsymbol{e} = \left[\left[\boldsymbol{e}_p\right]_{3\times3} \quad \left[\boldsymbol{e}_s\right]_{3\times2}\right] \tag{14}$$

in which V is electric potential while the electrical terminals are set as depicted in Fig. 1.

For the proposed ASP, the total energy Π is obtained from the in-plane work done by the temperature change and the strain energy. Therefore, Π is described as follows (Moradi-Dastjerdi and Behdinan, 2020a):

$$\Pi = \frac{1}{2}\int_V \left[\boldsymbol{\varepsilon}^T\boldsymbol{\sigma} - \boldsymbol{E}^T\boldsymbol{D}\right]dV + \frac{1}{2}\int_\Omega \left\{\left(w_{,x}\right)^2 + \left(w_{,y}\right)^2\right\} F d\Omega \tag{15}$$

where Ω and V are the side area and the volume of the ASP, respectively. F also is the in-plane load caused by a uniform change in the environment temperature ($\Delta T_r = T_r - 300$ where T_r is critical buckling temperature) and determined as follows (Moradi-Dastjerdi and Behdinan, 2020a):

$$F = \int_{-t/2}^{t/2} \boldsymbol{Q}_b \alpha \Delta T_r dz \tag{16}$$

3. Mesh-free solution

The details of obtaining the mesh-free form of governing buckling equation and its solution are presented in this section. At the first step, the unknowns of the displacement field **d** available in Eq. (6) are approximated at the scattered nodes in their effective domains. In this work, the generalized values of these unknowns are approximated using MLS shape functions χ as follows (Lancaster and Salkauskas 1981, Moradi-Dastjerdi and Behdinan 2020a):

$$\widehat{\boldsymbol{d}} = \left[\hat{u}_{0i}, \hat{v}_{0i}, \hat{w}_{0i}, \hat{\theta}_{xi}, \hat{\theta}_{yi}\right]^T = \sum_{i=1}^{n} \chi_i d_i \tag{17}$$

where n is node numbers. The concept of this approximation can also be applied in the estimation of electric potential at each node.

Then, the substitution of nodal values of displacement unknowns and electric potential into Eqs. (7) and (13) results in the mesh-free definitions of strain and electric field vectors as stated below:

$$\boldsymbol{\varepsilon}_b = \{\boldsymbol{\xi}_0 + z\boldsymbol{\xi}_1 + c_1 z^3 \boldsymbol{\xi}_3\}\widehat{\boldsymbol{d}}, \boldsymbol{\gamma} = (1 + 3c_1 z^2)\boldsymbol{\xi}_s \widehat{\boldsymbol{d}} \tag{18}$$

$$\boldsymbol{E} = -\boldsymbol{\xi}_e \widehat{\boldsymbol{V}} \tag{19}$$

where $\boldsymbol{\xi}_i$ (i = 0, 1, 3, s and e) are expressed in the Appendix.

Now, by substituting the mesh-free forms of displacement vector (Eq. 17), strain vectors (Eq. 18), potential electric vector (Eq. 19) and constitutive equation (Eq. 9) into the total energy function (Eq. 15), the new mesh-free form energy function will be obtained. Then, by taking derivation with respect to displacement and electric potential, the governing eigenvalue equations for the thermal behavior of the ASP will be obtained as follows:

$$\begin{bmatrix}\boldsymbol{K}_{uu} & \boldsymbol{K}_{ue}\\ \boldsymbol{K}_{eu} & -\boldsymbol{K}_{ee}\end{bmatrix}\begin{Bmatrix}\widehat{\boldsymbol{d}}\\ \widehat{\boldsymbol{V}}\end{Bmatrix} + \Delta T_r \begin{bmatrix}\boldsymbol{K}_{gg} & 0\\ 0 & 0\end{bmatrix}\begin{Bmatrix}\widehat{\boldsymbol{d}}\\ \widehat{\boldsymbol{V}}\end{Bmatrix} = \begin{Bmatrix}0\\0\end{Bmatrix} \tag{20}$$

where $\boldsymbol{K}$ shows the stiffness matrices in which the subscripts of *uu*, *ue* (or *eu*), *ee* and *gg* are used for mechanical, electromechanical, piezoelectric permittivity, and geometrical, respectively. These stiffness matrices are defined as below:

$$\boldsymbol{K}_{uu} = \int_\Omega [\boldsymbol{\xi}_0^T \quad \boldsymbol{\xi}_1^T \quad \boldsymbol{\xi}_3^T]\overline{\boldsymbol{Q_b}}[\boldsymbol{\xi}_0 \quad \boldsymbol{\xi}_1 \quad \boldsymbol{\xi}_3]^T d\Omega + \int_\Omega [\boldsymbol{\xi}_s^T \quad \boldsymbol{B}_s^T]\overline{\boldsymbol{Q_s}}[\boldsymbol{\xi}_s \quad \boldsymbol{\xi}_s]^T d\Omega \tag{21}$$

$$\boldsymbol{K}_{ue} = \boldsymbol{K}_{ue}^T = \int_\Omega [\boldsymbol{\xi}_0^T \quad \boldsymbol{\xi}_1^T \quad \boldsymbol{\xi}_3^T]\overline{\boldsymbol{E}_{be}}\boldsymbol{\xi}_v d\Omega + \int_\Omega [\boldsymbol{\xi}_s^T \quad \boldsymbol{\xi}_s^T]\overline{\boldsymbol{E}_{se}}\boldsymbol{\xi}_v d\Omega \tag{22}$$

$$\boldsymbol{K}_{ee} = \int_\Omega \left[\boldsymbol{\xi}_e^T \bar{\boldsymbol{k}} \boldsymbol{\xi}_e\right] d\Omega \tag{23}$$

$$\boldsymbol{K}_g = \int_\Omega \boldsymbol{\xi}_g^T \begin{bmatrix}F & 0\\ 0 & F\end{bmatrix}\boldsymbol{\xi}_g d\Omega \tag{24}$$

where

$$\overline{\boldsymbol{Q_b}} = \int_{-h/2}^{h/2}\begin{bmatrix}1 & z & c_1 z^3\\ & z^2 & c_1 z^4\\ Sym. & & c_1^2 z^6\end{bmatrix}\boldsymbol{Q}_b dz \ , \quad \overline{\boldsymbol{Q_s}} = \int_{-h/2}^{h/2}\begin{bmatrix}1 & 3c_1 z^2\\ 3c_1 z^2 & 9c_1^2 z^4\end{bmatrix}\boldsymbol{Q}_s dz \tag{25}$$

$$\overline{\boldsymbol{E}_{be}} = \int_{-h/2}^{h/2}\{1 \quad z \quad c_1 z^3\}^T \boldsymbol{e}_b dz \ , \quad \overline{\boldsymbol{E}_{se}} = \int_{-h/2}^{h/2}\{1 \quad 3c_1 z^2\}^T \boldsymbol{e}_s dz \tag{26}$$

$$\bar{\boldsymbol{k}} = \int_{-h/2}^{h/2} \boldsymbol{k} dz \tag{27}$$

After implementing the boundary conditions (edges' support) in Eq. (20), the solution of the resulting system of equations leads to the values of critical buckling temperature rise for the proposed APSs.

4. Results and discussions

The utilized materials of the proposed ASP, the analysis type, and the solution approach have been elaborated in previous sections. In this section, after examining the trustworthiness of the extended solution, new results for the critical buckling temperature rise of the proposed ASPs are presented. Regarding the materials used in the proposed ASP, the core layer is made of PMMA while the active face sheets are a mixture of ZnO NWs embedded in an Epoxy matrix. The following material properties have been attributed to the utilized materials:

Table 1 Convergence and accuracy study of the present critical buckling temperature rises ΔT_r of Al/Al_2O_3 plates with different FG patterns of material distributions

Node/Reference	λ_0 =0	λ_0 =0.5	λ_0 =1	λ_0 =2	λ_0 =5
5 × 5	164.27	94.13	77.14	67.66	68.41
10 × 10	169.02	96.53	79.06	69.47	70.55
15 × 15	172.82	98.27	80.51	71.06	72.77
20 × 20	175.37	99.59	81.62	72.16	74.07
25 × 25	176.78	100.35	82.26	72.78	74.75
FSDT (Zhao *et al*. 2009)	175.82	99.16	82.35	71.01	74.59
HSDT (Bateni *et al*. 2013)	180.30	102.23	83.84	74.30	76.50
FSDT (Yu *et al*. 2016)	180.13	102.12	83.75	74.23	76.45

Table 2 Comparison study on critical buckling temperature rises ΔT_r of square and rectangular FG ceramic (ZrO_2) / Metal (Ti 6Al 4V) sandwich plates

	λ_1 =0.5, b/a=1		λ_1 =2, b/a=1		λ_1 =0, b/a=3	
Solution	a/t = 10	a/t = 50	a/t = 10	a/t = 50	a/t = 10	a/t = 50
Present (25 × 25)	807.29	33.67	666.39	27.48	531.97	21.92
HSDT (Zenkour and Sobhy 2010)	809.25	33.76	666.87	27.54	533.93	22.00
FSDT (Zenkour and Sobhy 2010)	807.45	33.75	664.36	27.54	533.92	22.00
CPT (Zenkour and Sobhy 2010)	845.38	33.81	689.5	27.58	550.65	22.03

PMMA (Shen, 2011): $\rho = 1150 Kg/m^3$, α=45 (10^{-6}/*K*), *E*=2.5 *GPa*, υ=0.34

Epoxy (Berger *et al*. 2005, Yasmin *et al*. 2006): α=73 (10^{-6}/*K*), *E*=3.8 *GPa*, υ=0.34, $k_{11}= k_{22}= k_{33}=0.07965\times10^{-9}$ *F/m*

ZnO NW (Özgür *et al*. 2005, Mishra *et al*. 2017)**:** α_{11}=2.49 (10^{-6}/*K*), α_{22}=4.31 (10^{-6}/*K*), $e_{31}=e_{32}$=-0.573 C/m^2, e_{33}=1.32 C/m^2, $e_{24}=e_{15}$=-0.48 C/m^2, $k_{11}= k_{22}=0.0757\times10^{-9}$ *F/m*, $k_{33}=0.0903\times10^{-9}$ *F/m*, $Q_{11}= Q_{22}$=209.7 *GPa*, Q_{12}=121.1 *GPa*, $Q_{13}= Q_{23}$=105.1 *GPa*, $Q_{44}= Q_{55}$=42.47 *GP*

It is worth mentioning that we assumed that the material properties are not temperature dependent, and general buckling modes have been considered failure mode. Furthermore, uniform temperature changes have been considered. Therefore, the ASPs are stress-free at room temperature and it has no pseudo-static deformation (Setoodeh *et al*. 2012, Ansari *et al*. 2020).

4.1 Validation study

Examining the trustworthiness of the thermal buckling behavior of the newly proposed ASP has been performed in this section. Given the originality of the current work, we modeled plates made of an FG mixture of Al and Al_2O_3 which has been dealt with in Refs. (Zhao *et al*. 2009, Bateni *et al*. 2013, Yu *et al*. 2016) using the first- and higher-order shear deformation theories of plates (i.e., FSDT and HSDT). Table 1 shows the critical buckling temperature rise ΔT_r of such FG plates when they are square, fully clamped and the ratio of length to thickness is a/t=50. The results show that the present buckling temperature changes are properly converged such that the present ΔT_r have good agreements with the reported results especially those reported by Zhao (2009). It should be mentioned that λ_0 indicates a specific FG distribution of materials as those patterns are specified in the related references (Zhao *et al*. 2009, Bateni *et al*. 2013, Yu *et al*. 2016).

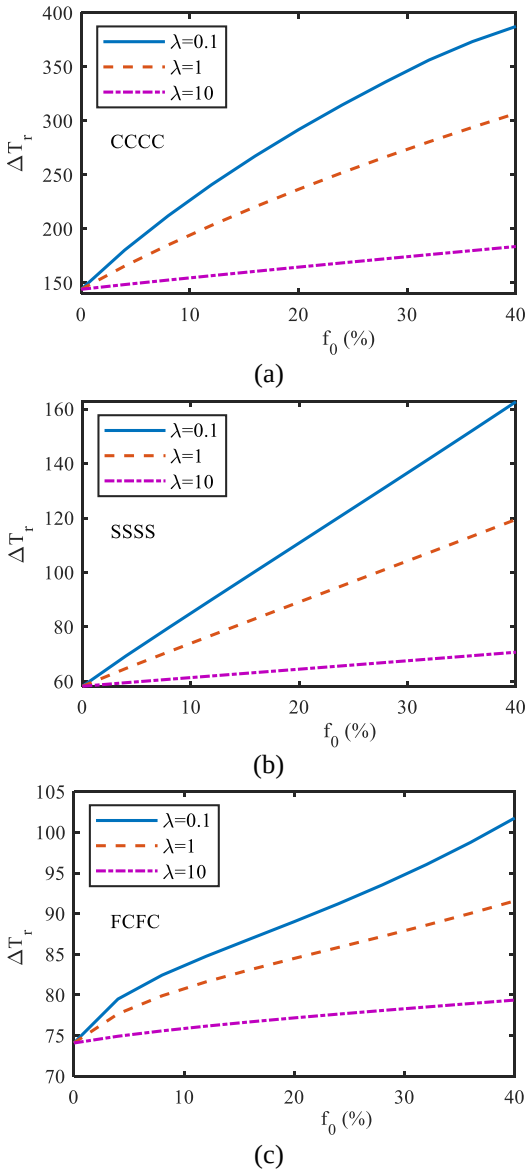

Fig. 2 critical buckling temperature rises of square (a) clamped (b) simply supported (c) FCFC APSs versus specific NW volume fraction for different patterns of NW distribution

As another comparison study, simply supported sandwich plates with a ceramic (ZrO_2) core and two FG ceramic (ZrO_2) / metal (Ti 6Al 4V) face sheets have been

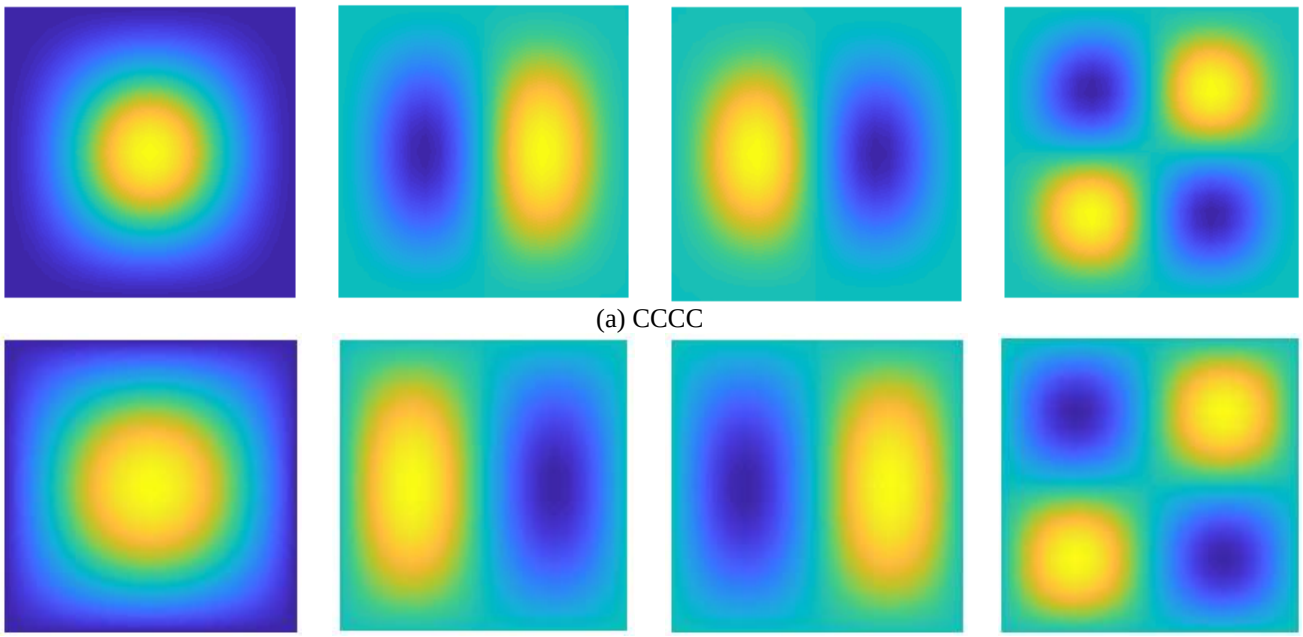

(a) CCCC

(b) SSSS

Fig. 3 first to fourth buckling mode shape of the square (a) clamped (b) simply supported APS

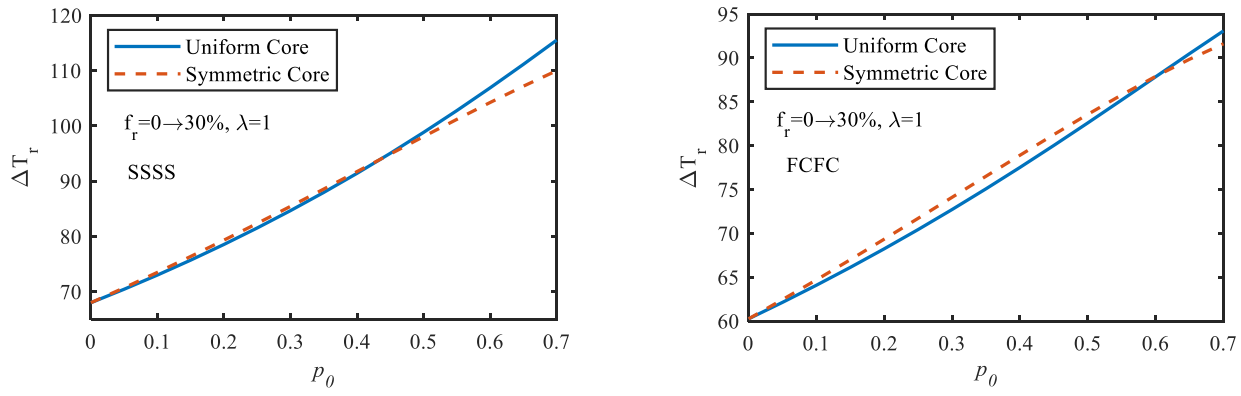

(a) (b)

Fig. 4 critical buckling temperature rises of square (a) simply supported (b) FCFC APSs versus porosity parameter for uniform and symmetric patterns of porosity distribution

considered as specifically described in (Zenkour and Sobhy 2010). Table 2 shows the critical buckling temperature rises of such square (b/a=1) and rectangular (b/a=3) sandwich plates for different patterns of material distributions shown by λ_1. The comparison between the obtained ΔT_r from the extended method in this work with those obtained from the classical plate theory (CPT), FSDT, and HSDT by (Zenkour and Sobhy 2010) shows a good agreement between results except those results obtained from CPL for thicker plates (a/t=10) which is due to the weakness of CPL for the solution of thick plates.

4.2 Thermal buckling resistance of the ASPs

This section characterizes the thermal buckling behavior of our proposed active sandwich plates. In the following examples, square simply supported APSs with a=0.3 m, t_c=0.01 m, t_p=0.001, $f_0 = 0.3$, $\lambda = 1, p_0$=0.6 (symmetric), and with open-circuit electrical terminals (as shown in Fig. 1) have been considered, unless it is mentioned.

To study the effect of ZnO NWs volume fraction and distribution patterns, APSs with various λ and f_0 have been considered. Fig. 2 shows ΔT_r for such APSs while they are fully clamped (CCCC), simply supported (SSSS) or two edges free and two edges clamped (FCFC). As shown, regardless of mechanical supports, increasing the amount of ZnO NW inside the matrix and/or distributing them on patterns with lower λ considerably improve buckling temperatures. This is because adding ZnO NWs into the Epoxy not only improves the elastic stiffness but also substantially reduces thermal expansion coefficients as the key factor in thermal buckling behaviors. Moreover, comparing the buckling temperatures of APSs with different boundary conditions discloses that clamped APSs have the highest while FCFC ones have the lowest ΔT_r. Fig. 3 illustrates the first to fourth buckling mode shapes of clamped and simply supported APSs.

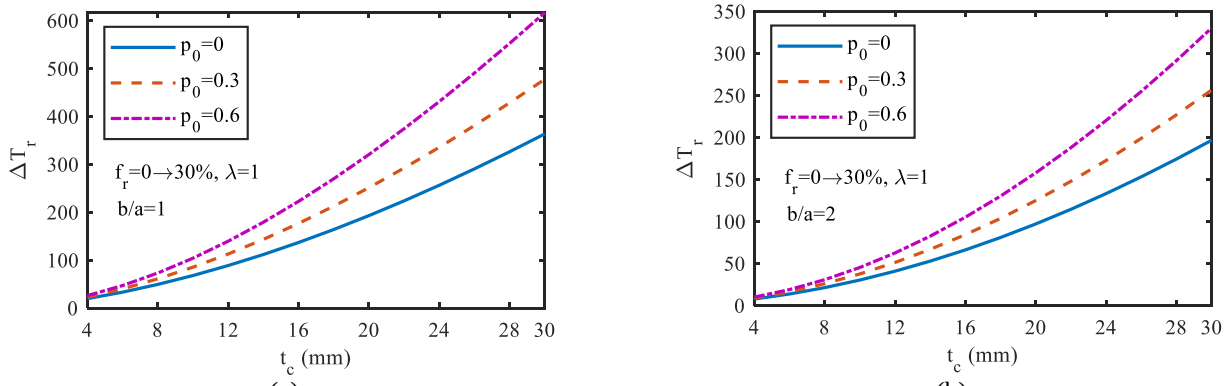

(a) (b)

Fig. 5 critical buckling temperature rises of (a) square (b) rectangular (b/a=2) simply supported APSs versus core thickness for different porosity amounts

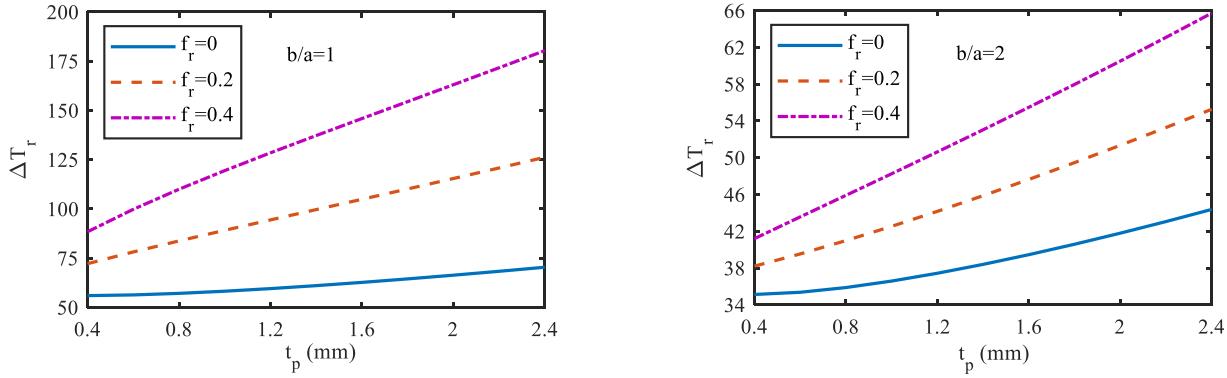

(a) (b)

Fig. 6 critical buckling temperature rises of (a) square (b) rectangular (b/a=2) simply supported APSs versus face sheet thickness for different NW amounts

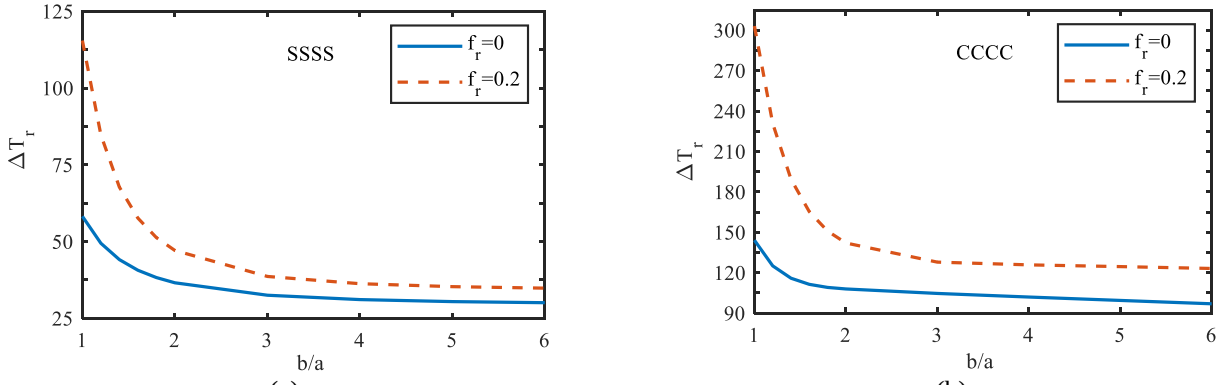

(a) (b)

Fig. 7 critical buckling temperature rises of (a) simply supported (b) clamped APSs versus core plates' aspect ratio for NW amounts

After the NW effect, porosity effects on the buckling temperature of the proposed APSs are studied. For FCFC and simply supported APSs with uniform and symmetric porosity distributions, Fig. 4 shows the ΔT_r versus porosity parameter. Interestingly, Fig. 4 discloses that adding more voids into the passive core layer significantly arises the buckling temperature of APSs due to lessening the thermal expansion of this layer and consequently the overall α of the APSs. It also observed that symmetric distribution of voids leads to higher ΔT_r in FCFC and simply supported APSs with up to p_0=0.6 and p_0=0.45, respectively. At those curve intersections i.e., p_0=0.6 for FCFC plates and p_0 =0.45 for SSSS plates, it can be concluded that the APSs with different void distributions have the same thermal buckling resistances.

The effect of core and face sheet thicknesses on the buckling temperature of the APSs are also investigated in Figs. 5 and 6, respectively. As shown in Fig. 5, the use of

thicker core sharply increases ΔT_r for both square and rectangular (b/a=2) APSs although square APSs have far higher critical buckling temperatures. Moreover, Fig. 5 reveals that porous APSs have higher buckling temperatures than APSs with a perfect core (p_0=0). Figure 6 also shows that increasing the thickness of active layers also dramatically increases critical buckling temperatures of the APSs where this increase is more considerable in APSs with higher amounts of ZnO NWs.

Finally, the effect of aspect ratio (b/a) of the APSs on ΔT_r is presented in Fig. 7 for plates with ($f_0 = 0.2$) and without ($f_0 = 0$) ZnO NWs in face sheets. Figures 7a and 7b plot ΔT_r versus the aspect ratio of simply supported and clamped APSs, respectively. They show that square APSs have the highest critical buckling temperature rise while simply supported APSs with $b/a > 5$ and clamped APSs with $b/a > 3$ have their lowest critical buckling temperatures. It is also observed that in APSs with ZnO NWs, ΔT_r and their lowest values (in rectangular APSs) are much higher than those of similar APSs without NWs ($f_0 = 0$).

5. Conclusions

An active lightweight sandwich plate made of lead-free piezoelectric face sheets integrating an FG porous polymeric core was proposed. By FG distributing piezoelectric NWs of ZnO in the face sheets, the whole structure was made electrically active which can be used as sensors/actuators or piezoelectric energy harvesters. Critical buckling temperature rises of the proposed structure were characterized by employing a higher-order plate theory to obtain the buckling eigenvalue system of equations. Moreover, using a mesh-free solution, the effects of controlling parameters of the ASP including porosity and ZnO volume and distribution, plate's supports, and plate's dimension on the critical buckling temperature rise were investigated. The results disclosed that adding ZnO NWs with f_0 =40% into the face sheets improves buckling temperature even more than double where the distribution of the nanowires also plays an important role. Moreover, it was observed that although the void distribution pattern does not have a considerable impact on the buckling temperature, incorporating 70% voids can improve the critical buckling temperatures by 70% for some specific APSs. Therefore, these results demonstrate the successful uses of ZnO NWs or voids in the sandwich structure where a lightweight and piezoelectrically active sandwich plate was proposed with a wide potential application. The main applications of the proposed active sandwich plates are using them as energy harvesters or sensors where the increase of ZnO NW provides a better coupling between electromechanical behavior of the structure and consequently, it improves the performance of those energy harvesters or sensors with ZnO NW/PDMS layer(s).

Acknowledgement

The authors are grateful for the financial support from the National Science and Technology Major Project of the Ministry of Science and Technology of the People's Republic of China (No.2012ZX04003101).

References

Ahmadi, H. and Foroutan, K. (2020), "Nonlinear static and dynamic thermal buckling analysis of imperfect multilayer FG cylindrical shells with an FG porous core resting on nonlinear elastic foundation", *J. Therm. Stress.*, **43**(5), 629-649. https://doi.org/10.1080/01495739.2020.1727802.

Akhras, G. and Li, W.C. (2010), "Three-dimensional thermal buckling analysis of piezoelectric antisymmetric angle-ply laminates using finite layer method", *Compos. Struct.*, **92**(1), 31-38. https://doi.org/10.1016/J.COMPSTRUCT.2009.06.010.

Alian, A.R., Kundalwal, S.I. and Meguid, S.A. (2015), "Multiscale modeling of carbon nanotube epoxy composites", *Polym.*, **70**, 149-160. https://doi.org/10.1016/j.polymer.2015.06.004.

Angelou, A., Norman, C., Miran, N., Albers, S., Moradi-Dastjerdi, R. and Behdinan, K. (2021), "An eco-friendly, biocompatible and reliable piezoelectric nanocomposite actuator for the new generation of microelectronic devices", *Eur. Phys. J. Plus*, **136**, 678. https://doi.org/10.1140/epjp/s13360-021-01653-z.

Ansari, E. and Setoodeh, A. (2019), "Applying isogeometric approach for free vibration, mechanical, and thermal buckling analyses of functionally graded variable-thickness blades", *Artic. J. Vib. Control*, **26**, 23-24. https://doi.org/10.1177/1077546320915336.

Ansari, E., Setoodeh, A.R. and Rabczuk, T. (2020), "Isogeometric-stepwise vibrational behavior of rotating functionally graded blades with variable thickness at an arbitrary stagger angle subjected to thermal environment", *Compos. Struct.*, **244**, 112281. https://doi.org/10.1016/j.compstruct.2020.112281.

Arshid, E., Amir, S. and Loghman, A. (2021a), "Bending and buckling behaviors of heterogeneous temperature-dependent micro annular/circular porous sandwich plates integrated by FGPEM nano-Composite layers", *J. Sandw. Struct. Mater.*, **23**(8), 3836 -3877. https://doi.org/10.1177/1099636220955027.

Arshid, E., Amir, S. and Loghman, A. (2021b), "Thermal buckling analysis of FG graphene nanoplatelets reinforced porous nanocomposite MCST-based annular/circular microplates", *Aerosp. Sci. Technol.*, **111**, 106561. https://doi.org/10.1016/J.AST.2021.106561.

Bateni, M., Kiani, Y. and Eslami, M.R. (2013), "A comprehensive study on stability of FGM plates", *Int. J. Mech. Sci.*, **75**, 134-44. https://doi.org/10.1016/j.ijmecsci.2013.05.014.

Behdinan, K. and Moradi-Dastjerdi, R. (2021), *Advanced Multifunctional Lightweight Aerostructures: Design, Development, and Implementation*, John Wiley & Sons.

Berger, H., Kari, S., Gabbert, U., Rodriguez-Ramos, R., Guinovart, R., Otero, J.A. and Bravo-Castillero, J. (2005), "An analytical and numerical approach for calculating effective material coefficients of piezoelectric fiber composites", *Int. J. Solids Struct.*, **42**(21-22), 5692-5714. https://doi.org/10.1016/j.ijsolstr.2005.03.016.

Bouazza, M. and Zenkour, A.M. (2020), "Hygro-thermo-mechanical buckling of laminated beam using hyperbolic refined shear deformation theory", *Compos. Struct.*, **252**, 112689. https://doi.org/10.1016/J.COMPSTRUCT.2020.112689.

Cetkovic, M. (2016), "Thermal buckling of laminated composite plates using layerwise displacement model", *Compos. Struct.*, **142**, 238-253. https://doi.org/10.1016/j.compstruct.2016.01.082.

Cong, P.H., Chien, T.M., Khoa, N.D. and Duc, N.D. (2018), "Nonlinear thermomechanical buckling and post-buckling response of porous FGM plates using Reddy's HSDT", *Aerosp. Sci. Technol.*, **77**, 419-428. https://doi.org/10.1016/j.ast.2018.03.020.

Dinh Khoa, N., Thi Thiem, H. and Duc, N.D. (2019), "Nonlinear buckling and postbuckling of imperfect piezoelectric S-FGM circular cylindrical shells with metal-ceramic-metal layers in thermal environment using Reddy's third-order shear deformation shell theory", *Mech. Adv. Mater. Struct.*, **26**(3), 248-259. https://doi.org/10.1080/15376494.2017.1341583.

Ebrahimi, F., Barati, M.R., Ebrahimi, F. and Barati, M.R. (2016), "An exact solution for buckling analysis of embedded piezo-electro-magnetically actuated nanoscale beams", *Adv. Nano Res.*, **4**(2), 65-84. https://doi.org/10.12989/ANR.2016.4.2.065.

Ebrahimi, F., Barati, M.R., Ebrahimi, F. and Barati, M.R. (2018), "Stability analysis of functionally graded heterogeneous piezoelectric nanobeams based on nonlocal elasticity theory", *Adv. Nano Res.*, **6**(2), 93-112. https://doi.org/10.12989/ANR.2018.6.2.093.

Fan, F., Cai, X., Sahmani, S. and Safaei, B. (2021), "Isogeometric thermal postbuckling analysis of porous FGM quasi-3D nanoplates having cutouts with different shapes based upon surface stress elasticity", *Compos. Struct.*, **262**, 113604. https://doi.org/10.1016/J.COMPSTRUCT.2021.113604.

Foroutan, M. and Moradi-Dastjerdi, R. (2011), "Dynamic analysis of functionally graded material cylinders under an impact load by a mesh-free method", *Acta Mech.*, **219**, 281-290. https://doi.org/10.1007/s00707-011-0448-4.

Ghahramani, P., Behdinan, K., Moradi-Dastjerdi, R. and Naguib, H.E. (2022), "Theoretical and experimental investigation of MWCNT dispersion effect on the elastic modulus of flexible PDMS / MWCNT nanocomposites", *Nanotechnol. Rev.*, **11**, 55-64. Available at: https://doi.org/10.1515/ntrev-2022-0006.

Heidari, F., Afsari, A., Janghorban, M., Heidari, F., Afsari, A. and Janghorban, M. (2020), "Several models for bending and buckling behaviors of FG-CNTRCs with piezoelectric layers including size effects", *Adv. Nano Res.*, **9**(3), 193-210. https://doi.org/10.12989/ANR.2020.9.3.193.

Jabbari, M., Hashemitaheri, M., Mojahedin, A. and Eslami, M.R. (2014), "Thermal buckling analysis of functionally graded thin circular plate made of saturated porous materials", *J. Therm. Stress.*, **37**(2), 202-220. https://doi.org/10.1080/01495739.2013.839768.

Kamarian, S., Bodaghi, M. and Song, J. (2020), "Hygrothermal effects on the buckling of soft-core sandwich plates with composite layered face sheets", *Polym. Compos.*, **41**(10), 4144-4169. https://doi.org/10.1002/PC.25700.

Kamarian, S., Bodaghi, M., Isfahani, R.B. and Song, J.I. (2021), "Thermal buckling analysis of sandwich plates with soft core and CNT-Reinforced composite face sheets", *J. Sandw. Struct. Mater.*, **23**(8), 3606-3644. https://doi.org/10.1177/1099636220935557.

Keshmiri, A., Wu, N. and Wang, Q. (2018), "A new nonlinearly tapered FGM piezoelectric energy harvester", *Eng. Struct.*, **173**, 52-60. https://doi.org/10.1016/j.engstruct.2018.06.081.

Kundalwal, S.I. and Ray, M.C. (2016), "Smart damping of fuzzy fiber reinforced composite plates using 1-3 piezoelectric composites", *J. Vib. Control*, **22**(6), 1526-1546. https://doi.org/10.1177/1077546314543726.

Lancaster, P. and Salkauskas, K. (1981), "Surface Generated by Moving Least Squares Methods", *Math. Comput.*, **37**, 141-158.

Malekzadeh, P., Setoodeh, A.R. and Beni, A.A. (2011), "Small scale effect on the thermal buckling of orthotropic arbitrary straight-sided quadrilateral nanoplates embedded in an elastic medium", *Compos. Struct.*, **93**(8), 2083-2089. https://doi.org/10.1016/J.COMPSTRUCT.2011.02.013.

Malekzadeh, P., Setoodeh, A.R. and Shojaee, M. (2018), "Vibration of FG-GPLs eccentric annular plates embedded in piezoelectric layers using a transformed differential quadrature method", *Comput. Methods Appl. Mech. Eng.*, **340**, 451-479. https://doi.org/10.1016/j.cma.2018.06.006.

Mehar, K., Panda, S.K., Mehar, K. and Panda, S.K. (2019), "Multiscale modeling approach for thermal buckling analysis of nanocomposite curved structure", *Adv. Nano Res.*, **7**(3), 181-190. https://doi.org/10.12989/ANR.2019.7.3.181.

Mekerbi, M., Benyoucef, S., Mahmoudi, A., Bourada, F. and Tounsi, A. (2019), "Investigation on thermal buckling of porous FG plate resting on elastic foundation via quasi 3D solution", *Struct. Eng. Mech.*, **72**(4), 513-524. https://doi.org/10.12989/SEM.2019.72.4.513.

Meschino, M., Wang, L., Xu, H., Moradi-Dastjerdi, R. and Behdinan, K. (2021), "Low-frequency nanocomposite piezoelectric energy harvester with embedded zinc oxide nanowires", *Polym. Compos.*, **42**, 4573-4585. https://doi.org/10.1002/pc.26169.

Mirjavadi, S.S., Matin, A., Shafiei, N., Rabby, S., Behzad, Afshari, M., Sajad Mirjavadi, S., Shaaei, N. and Afshari, B.M. (2017), "Thermal buckling behavior of two-dimensional imperfect functionally graded microscale-tapered porous beam", *J. Therm. Stress.*, **40**(10), 1201-1214. https://doi.org/10.1080/01495739.2017.1332962.

Mirzaei, M. and Kiani, Y. (2017), "Isogeometric thermal buckling analysis of temperature dependent FG graphene reinforced laminated plates using NURBS formulation", *Compos. Struct.*, **180**, 606-16. https://doi.org/10.1016/j.compstruct.2017.08.057.

Mishra, N., Krishna, B., Singh, R. and Das, K. (2017), "Evaluation of effective elastic, piezoelectric, and dielectric properties of SU8/ZnO nanocomposite for vertically integrated nano-generators using finite element method", *J. Nanomater.*, **2017**, 1924651. https://doi.org/10.1155/2017/1924651.

Moradi-Dastjerdi, R. and Behdinan, K. (2020a), "Stability analysis of multifunctional smart sandwich plates with graphene nanocomposite and porous layers", *Int. J. Mech. Sci.*, **167**, 105283. https://doi.org/10.1016/j.ijmecsci.2019.105283.

Moradi-Dastjerdi, R. and Behdinan, K. (2020b), "Thermo-electro-mechanical behavior of an advanced smart lightweight sandwich plate", *Aerosp. Sci. Technol.*, **106**, 106142. https://doi.org/10.1016/j.ast.2020.106142.

Moradi-Dastjerdi, R. and Behdinan, K. (2021a), "Dynamic performance of piezoelectric energy harvesters with a multifunctional nanocomposite substrate", *Appl. Energy*, **293**, 116947. https://doi.org/10.1016/j.apenergy.2021.116947.

Moradi-Dastjerdi, R. and Behdinan, K. (2021b), "Free vibration response of smart sandwich plates with porous CNT-reinforced and piezoelectric layers", *Appl. Math. Model.*, **96**, 66-79. https://doi.org/10.1016/j.apm.2021.03.013.

Moradi-Dastjerdi, R. and Behdinan, K. (2021c), "Stress waves in thick porous graphene-reinforced cylinders under thermal gradient environments", *Aerosp. Sci. Technol.*, **110**, 106476. https://doi.org/10.1016/j.ast.2020.106476.

Moradi-Dastjerdi, R. and Behdinan, K. (2021d), "Temperature effect on free vibration response of a smart multifunctional sandwich plate", *J. Sandw. Struct. Mater.*, **23**(6), 2399-2421. Available at: https://doi.org/10.1177/1099636220908707.

Moradi-Dastjerdi, R., Radhi, A. and Behdinan, K. (2020), "Damped dynamic behavior of an advanced piezoelectric sandwich plate", *Compos. Struct.*, **243**, 112243. https://doi.org/10.1016/j.compstruct.2020.112243.

Mosallaie Barzoki, A.A., Ghorbanpour Arani, A., Kolahchi, R. and Mozdianfard, M.R. (2012), "Electro-thermo-mechanical torsional buckling of a piezoelectric polymeric cylindrical shell reinforced by DWBNNTs with an elastic core", *Appl. Math. Model.*, **36**(7), 2983-2995. https://doi.org/10.1016/j.apm.2011.09.093.

Nguyen, L.B., Nguyen, N.V, Thai, C.H., Ferreira, A.M.J. and Nguyen-xuan, H. (2019), "An isogeometric Bézier finite element analysis for piezoelectric FG porous plates reinforced by graphene platelets", *Compos. Struct.*, **214**, 227-245.

https://doi.org/10.1016/j.compstruct.2019.01.077.
Özgür, Ü., Alivov, Y.I., Liu, C., Teke, A., Reshchikov, M.A., Doğan, S., Avrutin, V., Cho, S.J. and Morkoç, H. (2005), "A comprehensive review of ZnO materials and devices", *J. Appl. Phys.*, 1-103. https://doi.org/10.1063/1.1992666.
Pan, S., Dai, Q., Safaei, B., Qin, Z. and Chu, F. (2021), "Damping characteristics of carbon nanotube reinforced epoxy nanocomposite beams", *Thin-Walled Struct.*, **166**, 108127. https://doi.org/10.1016/J.TWS.2021.108127.
Polit, O., Anant, C., Anirudh, B. and Ganapathi, M. (2019), "Functionally graded graphene reinforced porous nanocomposite curved beams: Bending and elastic stability using a higher-order model with thickness stretch effect", *Compos. Part B*, **166**(December 2018), 310-327. https://doi.org/10.1016/j.compositesb.2018.11.074.
Reddy, J.N. (2004), *Mechanics of Laminated Composite Plates and Shells: Theory and Analysis*, CRC press.
Safaei, B. (2021), "Frequency-dependent damped vibrations of multifunctional foam plates sandwiched and integrated by composite faces", *Eur. Phys. J. Plus*, **136**, 646. https://doi.org/10.1140/epjp/s13360-021-01632-4.
Setoodeh, A.R., Ghorbanzadeh, M. and Malekzadeh, P. (2012), "A two-dimensional free vibration analysis of functionally graded sandwich beams under thermal environment", *Proc. Inst. Mech. Eng. Part C J. Mech. Eng. Sci.*, **226**(12), 2860-2873. https://doi.org/10.1177/0954406212440669.
Setoodeh, A.R., Shojaee, M. and Malekzadeh, P. (2018), "Application of transformed differential quadrature to free vibration analysis of FG-CNTRC quadrilateral spherical panel with piezoelectric layers", *Comput. Methods Appl. Mech. Engrg.*, **335**, 510-537. https://doi.org/10.1016/j.cma.2018.02.022.
Setoodeh, A.R., Shojaee, M. and Malekzadeh, P. (2019), "Vibrational behavior of doubly curved smart sandwich shells with FG-CNTRC face sheets and FG porous core", *Compos. Part B Eng.*, **165**, 798-822. https://doi.org/10.1016/J.COMPOSITESB.2019.01.022.
Shen, H.S. (2011), "Postbuckling of nanotube-reinforced composite cylindrical shells in thermal environments, Part I : Axially-loaded shells", *Compos. Struct.*, **93**(8), 2096-2108. https://doi.org/10.1016/j.compstruct.2011.02.011.
Singh, S., Singh, J. and Shukla, K.K. (2013), "Buckling of laminated composite plates subjected to mechanical and thermal loads using meshless collocations", *J. Mech. Sci. Technol.*, **27**(2), 327-336. https://doi.org/10.1007/s12206-012-1249-y.
Sobhani, E. and Masoodi, A.R. (2021), "Natural frequency responses of hybrid polymer/carbon fiber/FG-GNP nanocomposites paraboloidal and hyperboloidal shells based on multiscale approaches", *Aerosp. Sci. Technol.*, **119**, 107111. https://doi.org/10.1016/J.AST.2021.107111.
Sobhani, E., Masoodi, A.R. and Ahmadi-Pari, A.R. (2021), "Vibration of FG-CNT and FG-GNP sandwich composite coupled Conical-Cylindrical-Conical shell", *Compos. Struct.*, **273**, 114281. https://doi.org/10.1016/J.COMPSTRUCT.2021.114281.
Sobhani, E., Masoodi, A.R., Civalek, O. and Ahmadi-Pari, A.R. (2022a), "Agglomerated impact of CNT vs. GNP nanofillers on hybridization of polymer matrix for vibration of coupled hemispherical-conical-conical shells", *Aerosp. Sci. Technol.*, **120**, 107257. https://doi.org/10.1016/J.AST.2021.107257.
Sobhani, E., Moradi-Dastjerdi, R., Behdinan, K., Masoodi, A.R. and Ahmadi-Pari, A.R. (2022b), "Multifunctional trace of various reinforcements on vibrations of three-phase nanocomposite combined hemispherical-cylindrical shells", *Compos. Struct.*, **279**, 114798. https://doi.org/10.1016/j.compstruct.2021.114798.
Sobhy, M. and Zenkour, A.M. (2018), "Nonlocal Thermal and Mechanical Buckling of Nonlinear Orthotropic Viscoelastic Nanoplates Embedded in a Visco-Pasternak Medium", *Int. J. Appl. Mech.*, **10**(8), 1850086. https://doi.org/10.1142/S1758825118500862.
Sobhy, M. (2021), "Analytical buckling temperature prediction of FG piezoelectric sandwich plates with lightweight core", *Mater. Res. Express*, **8**, 95704. https://doi.org/10.1088/2053-1591/ac28b9.
Tan, P. and Tong, L. (2001), "Micro-electromechanics models for piezoelectric-fiber-reinforced composite materials", *Compos. Sci. Technol.*, **61**(5), 759-769. https://doi.org/10.1016/S0266-3538(01)00014-8.
Tao, C. and Dai, T. (2022), "Modified couple stress-based nonlinear static bending and transient responses of size-dependent sandwich microplates with graphene nanocomposite and porous layers", *Thin-Walled Struct.*, **171**, 108704. https://doi.org/10.1016/J.TWS.2021.108704.
Tounsi, A., Benguediab, S., Bedia, E.A.A., Semmah, A., Zidour, M., Tounsi, A., Benguediab, S., Bedia, E.A.A., Semmah, A. and Zidour, M. (2013), "Nonlocal effects on thermal buckling properties of double-walled carbon nanotubes", *Adv. Nano Res.*, **1**(1), 1-11. https://doi.org/10.12989/ANR.2013.1.1.001.
Trinh, M.C. and Kim, S.E. (2019), "Nonlinear stability of moderately thick functionally graded sandwich shells with double curvature in thermal environment", *Aerosp. Sci. Technol.*, **84**, 672-685. https://doi.org/10.1016/j.ast.2018.09.018.
Tuloup, C., Harizi, W., Aboura, Z., Meyer, Y., Khellil, K. and Lachat, R. (2019), "On the use of in-situ piezoelectric sensors for the manufacturing and structural health monitoring of polymer-matrix composites: A literature review", *Compos. Struct.*, **215**, 127-149. https://doi.org/10.1016/J.COMPSTRUCT.2019.02.046.
Wang, E., Tehrani, M.S., Zare, Y. and Rhee, K.Y. (2018), "A new methodology based on micromechanics model to predict the tensile modulus and network formation in polymer/CNT nanocomposites", *Colloid Surface A*, **550**, 20-26. https://doi.org/10.1016/j.colsurfa.2018.04.032.
Yaghoobi, H., Fereidoon, A., Khaksari Nouri, M. and Mareishi, S. (2015), "Thermal buckling analysis of piezoelectric functionally graded plates with temperature-dependent properties", *Mech. Adv. Mater. Struct.*, **22**(10), 864-875. https://doi.org/10.1080/15376494.2013.864436.
Yang, Z., Liu, A., Lai, S.K., Safaei, B., Lv, J., Huang, Y. and Fu, J. (2022), "Thermally induced instability on asymmetric buckling analysis of pinned-fixed FG-GPLRC arches", *Eng. Struct.*, **250**, 113243. https://doi.org/10.1016/J.ENGSTRUCT.2021.113243.
Yasmin, A., Luo, J.J., Abot, J.L. and Daniel, I.M. (2006), "Mechanical and thermal behavior of clay/epoxy nanocomposites", *Compos. Sci. Technol.*, **66**(14), 2415-2422. https://doi.org/10.1016/j.compscitech.2006.03.011.
Yu, T., Quoc Bui, T., Yin, S., Doan, H., Wu, C.T., Van Do, T. and Tanaka, S. (2016), "On the thermal buckling analysis of functionally graded plates with internal defects using extended isogeometric analysis", *Compos. Struct.*, **136**, 684-695. https://doi.org/10.1016/j.compstruct.2015.11.002.
Zargar, O., Mollaghaee-Roozbahani, M., Bashirpour, M. and Baghani, M. (2019), "The application of Homotopy Analysis Method to determine the thermal response of convective-radiative porous fins with temperature-dependent properties", *Int. J. Appl. Mech.* https://doi.org/10.1142/s1758825119500881.
Zenkour, A.M. and Sobhy, M. (2010), "Thermal buckling of various types of FGM sandwich plates", *Compos. Struct.*, **93**(1), 93-102. https://doi.org/10.1016/J.COMPSTRUCT.2010.06.012.
Zenkour, A.M. and Aljadani, M.H. (2019), "Porosity effect on thermal buckling behavior of actuated functionally graded piezoelectric nanoplates", *Eur. J. Mech. A/Solids*, **78**, 103835. https://doi.org/10.1016/j.euromechsol.2019.103835.
Zhang, L., Zhang, F., Qin, Z., Han, Q., Wang, T. and Chu, F.

(2022), "Piezoelectric energy harvester for rolling bearings with capability of self-powered condition monitoring", *Energy*, **238**, 121770. https://doi.org/10.1016/J.ENERGY.2021.121770.

Zhao, X., Lee, Y.Y. and Liew, K.M. (2009), "Mechanical and thermal buckling analysis of functionally graded plates", *Compos. Struct.*, **90**, 161-171. https://doi.org/10.1016/j.compstruct.2009.03.005.

Zhao, S., Zhao, Z., Yang, Z., Ke, L.L., Kitipornchai, S. and Yang, J. (2020), "Functionally graded graphene reinforced composite structures: A review", *Eng. Struct.*, 110339. https://doi.org/10.1016/j.engstruct.2020.110339.

Appendix

$$\boldsymbol{\xi}_e = [0 \quad 0 \quad 1/t_p] \tag{A1}$$

$$\boldsymbol{\xi}_g = \begin{bmatrix} 0 & 0 & \chi_{i,x} & 0 & 0 \\ 0 & 0 & \chi_{i,y} & 0 & 0 \end{bmatrix} \tag{A2}$$

$$\begin{aligned} \boldsymbol{\xi}_0 &= \begin{bmatrix} \chi_{i,x} & 0 & 0 & 0 & 0 \\ 0 & \chi_{i,y} & 0 & 0 & 0 \\ \chi_{i,y} & \chi_{i,x} & 0 & 0 & 0 \end{bmatrix}, \\ \boldsymbol{\xi}_1 &= \begin{bmatrix} 0 & 0 & 0 & \chi_{i,x} & 0 \\ 0 & 0 & 0 & 0 & \chi_{i,y} \\ 0 & 0 & 0 & \chi_{i,y} & \chi_{i,x} \end{bmatrix}, \\ \boldsymbol{\xi}_3 &= \begin{bmatrix} 0 & 0 & \chi_{i,xx} & \chi_{i,x} & 0 \\ 0 & 0 & \chi_{i,yy} & 0 & \chi_{i,y} \\ 0 & 0 & 2\chi_{i,xy} & \chi_{i,y} & \chi_{i,x} \end{bmatrix}, \\ \boldsymbol{\xi}_s &= \begin{bmatrix} 0 & 0 & \chi_{i,x} & \chi_i & 0 \\ 0 & 0 & \chi_{i,y} & 0 & \chi_i \end{bmatrix} \end{aligned} \tag{A3}$$